Changes of cell growth and magnetosome biomineralization in *Magnetospirillum magneticum* AMB-1 after ultraviolet-B irradiation

Yinzhao Wang[1,2], Wei Lin[1,2], Jinhua Li[1,2] and Yongxin Pan[1,2]*

[1] Biogeomagnetism Group, Paleomagnetism and Geochronology Laboratory, Key Laboratory of the Earth's Deep Interior, Institute of Geology and Geophysics, Chinese Academy of Sciences, Beijing, China

[2] France-China Bio-Mineralization and Nano-Structures Laboratory, Chinese Academy of Sciences, Beijing, China

Effects of ultraviolet radiation on microorganisms are of great interest in field of microbiology and planetary sciences. In the present study, we used *Magnetospirillum magneticum* AMB-1 as a model organism to examine the influence of ultraviolet-B (UV-B) radiation on cell growth and magnetite biomineralization of magnetotactic bacteria (MTB). Live AMB-1 cells were exposed to UV-B radiation for 60, 300 and 900 s, which correspond to radiation doses of $120\,J/m^2$, $600\,J/m^2$, and $1800\,J/m^2$, respectively. After irradiation, the amounts of cyclobutane pyrimidine dimers (CPD) and reactive oxygen species (ROS) of the cells were increased, and cell growth was stunted up to ~170 h, depending on the UV-B radiation doses. The UV-B irradiated cells also produced on average more magnetite crystals with larger grain sizes and longer chains, which results in changes of their magnetic properties.

Keywords: magnetotactic bacteria, ultraviolet-B radiation, cell growth, microbial biomineralization, rock magnetic measurement

INTRODUCTION

Solar ultraviolet radiation (wavelengths 10-400 nm) fluctuation is proposed as one of the most important selective pressures on the evolution of life on Earth (Cockell, 1998; Garcia-Pichel, 1998; Häder et al., 2007; Sinha and Häder, 2008; Weigand and Sundin, 2012). Although the stratospheric ozone protects organisms on Earth from UV radiation exposure (Solomon, 1999), the ozone layer can be stripped away by solar wind when the strength of the Earth's magnetic field is low. For instance, during geomagnetic excursion or polarity reversal, the field is thought to 20% of its typical strength (Reid and Isaksen, 1976; McKenzie et al., 2003; Glassmeier and Vogt, 2010; Stadelmann et al., 2010; Valet and Valladas, 2010). Consequently, the depletion of the ozone layer will lead to increased penetration of harmful radiation to the Earth's surface, which may affect aquatic ecosystems (Hargreaves, 2003; Wulff et al., 2008). UV-C radiation (wavelengths 10–280 nm) can normally be absorbed by the ozone layer, but UV-B (wavelengths 280–320 nm) and UV-A radiation (wavelengths 320–400 nm) can reach the biosphere and influence living organisms (Zepp et al., 1998; Zenoff et al., 2006; Konhauser et al., 2007; Santos et al., 2013). In addition to enhancing production of intracellular reactive oxygen species (ROS) (similar to the UV-A radiation), UV-B radiation could directly damage DNA in organisms and thus should be more detrimental to organism health (Qiu et al., 2005b; Hernandez et al., 2006; Santos et al., 2013).

Microorganisms are the earliest known species to have appeared on Earth. Various microorganisms could form minerals and thus can leave fossil records that have been used to trace early life on Earth and other planets such as Mars (Li et al., 2013a). However, how UV radiation influences the microbial biomineralization and the formation of fossil biominerals or mineral-encrusted cells (i.e., microfossils) is still poorly understood (Cockell, 1998; Garcia-Pichel, 1998; Häder et al., 2007; Singh et al., 2010). Recent investigations on aquatic bacterial isolates have revealed that UV-B radiation could lead to DNA lesion and cellular oxidative stress (Agogué et al., 2005; Santos et al., 2011, 2012, 2013; Matallana-Surget et al., 2012; Singh et al., 2012). On the other hand, some microorganisms have evolved strategies to mitigate such irradiation damage (Sinha and Häder, 2008; Schmidt et al., 2009; Weigand and Sundin, 2009; Singh et al., 2010; Weigand et al., 2011). For example, *in vitro* biomineralization of iron-silica biominerals of filamentous cyanobacterium *Calothrix* help the bacteria efficiently coping with UV irradiation. Compared with non-mineralized bacteria, the mineralized bacteria represent remarkable resistance to UV irradiation as revealed by the rates of photosynthesis, chlorophyll-a content, and phycocyanin autofluorescence (Phoenix et al., 2001). Cyanobacterium *Lyngbya majuscula* was found to produce chemical compounds that were able to absorb UV radiation and synthesize an incrassate cell sheath under enhanced UV-B irradiation (Mandal et al., 2011).

Magnetotactic bacteria (MTB) are able to synthesis single domain (SD) magnetic particles within intracellular membrane organelles called magnetosome (Bazylinski and Frankel, 2004; Faivre and Schüler, 2008). The magnetosome, usually arranged in chain(s), facilitate MTB to navigate along the Earth's magnetic field and efficiently find the optimal living conditions in aquatic and sedimentary environments, a process known as magnetotaxis (Bazylinski and Frankel, 2004; Pan et al., 2009). After MTB die and are buried, the magnetosome crystals can be preserved as

fossil biominerals (magnetofossils), which are potential geological records for paleoenvironmental and paleomagnetic information, as well as biosignatures for searching early life on Earth and extraterrestrial life (Petersen et al., 1986; Chang and Kirschvink, 1989; McKay et al., 1996; Yamazaki and Kawahata, 1998; Arató et al., 2005; Pan et al., 2005; Kopp and Kirschvink, 2008; Paterson et al., 2013). Previous studies have demonstrated that environmental factors, such as salinity, temperature, the strength of geomagnetic field, oxygen and iron resource, can influence the overall diversity of MTB communities in nature and the compositional, physical, and magnetic features of magnetosomes (e.g., Lins et al., 2007; Faivre et al., 2008; Lin et al., 2011, 2013a,b; Li and Pan, 2012; Wang et al., 2013). However, to our knowledge, the influence of UV radiation on MTB has not been studied yet, although it is of particular interest for better understanding the evolution of magnetotaxis in early history of Earth. During a geomagnetic excursion or polarity reversal, where the dipolar geomagnetic field was weak and the UV radiation was strong, how MTB respond to the environmental changes also remains unknown. In the present study, we have investigated the effects of UV-B radiation on cell growth and magnetite biomineralization of *Magnetospirillum magneticum* AMB-1. Possible relationships between magnetosome formation and UV-B irradiation are discussed.

MATERIALS AND METHODS

PREPARATION OF CELL AND GROWTH CONDITIONS

A facultative anaerobic MTB strain *Magnetospirillum magneticum* AMB-1 (ATCC700264) was used in this study. In all experiments, cells were cultivated in the magnetic spirillum growth medium (MSGM) (Blakemore et al., 1979). This medium (1 L) contains 5 ml of Wolfe's mineral solution, 10 ml of Wolfe's vitamin solution, 0.68 g of potassium phosphate, 0.12 g of sodium nitrate, 0.05 g of sodium acetate, 0.035 g of ascorbic acid, 0.37 g of tartaric acid, 0.37 g of succinic acid, and 50 μM of ferric quinate. In order to obtain a uniform genotype strain, originally activated AMB-1 cells were plated onto MSGM agar plate for 7 days, single clone was picked up and enlarged cultivated for the following studies. Non-magnetic AMB-1 cells were obtained by growing cells under 220 rpm rotation at 26°C with free air exchange. The non-magnetic cells were then inoculated equally to twelve UV-B penetrable quartz bottles. Each bottle contained 300 mL of MSGM culture medium and was incubated under the same cultivation condition. When the cell density reached $\sim 1.0 \times 10^7$ cells/ml at early exponent phase, the bottle was used for the irradiation experiment.

SOURCE OF UV-B RADIATION AND IRRADIATION EXPERIMENT

The irradiation experiment system is shown in **Figure 1**. UV-B radiation was obtained from USHIO ultraviolet lamps (USHIO America, USA). The lamps were coated with special blended phosphor to emit radiation peaking at 306 nm. The radiation intensity of light source was measured by a double-channel UV-B radiometer with a detective range between 275 and 330 nm (Beijing Normal University, China). The double-sided UV-B irradiation system with an averaged UV-B radiation intensity of 2.0 W/m^2 was used to carry out the experiment. The irradiation
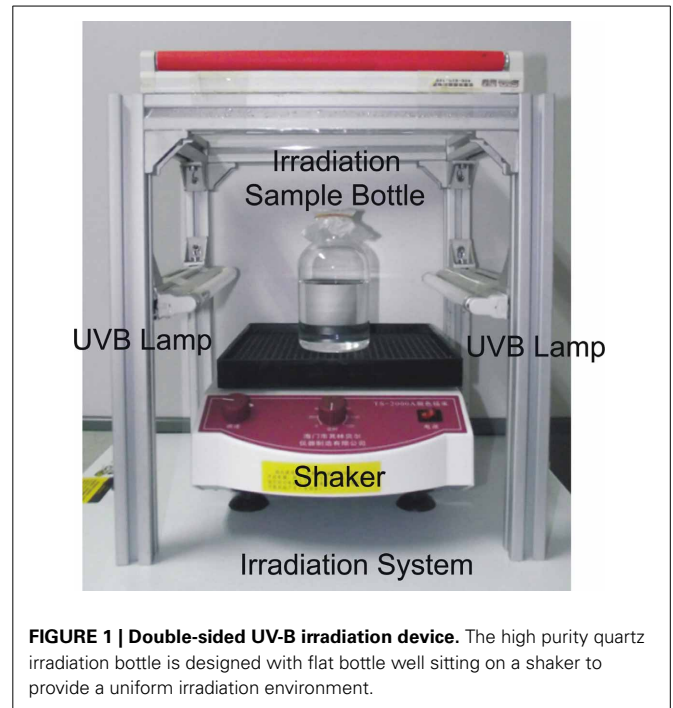

FIGURE 1 | Double-sided UV-B irradiation device. The high purity quartz irradiation bottle is designed with flat bottle well sitting on a shaker to provide a uniform irradiation environment.

bottles containing AMB-1 inoculations were exposed to UV-B radiation for 60, 300, and 900 s, which were equivalent to radiation doses of 120, 600, and 1800 J/m^2, respectively. To ensure even exposure the bottles were rotated at 50 rpm during irradiation. Non-irradiated cell samples (bottles covered with aluminum foils) were taken as experimental control. All twelve irradiation bottles with AMB-1 cells were divided into the four different experiment groups with tripled repeats of each UV-B radiation condition.

After the irradiation, 10 mL of cells were immediately taken from the bottle for cyclobutane pyrimidine dimers (CPD) and ROS analyses. The rest of the culture was centrifuged at 4°C 6000 rpm for 10 min. Then the cells of each sample were washed by 0.9% NaCl (wt/vol) and inoculated into 500-mL fresh MSGM medium, respectively under anaerobic condition in the dark. The cell growth of each group was examined through the optical density at 600 nm (OD$_{600}$). As the sample reached stationary phase for 40 h, the cells were harvested for cell morphology, magnetosome crystal, and magnetic analyses.

DETERMINATION OF RELATIVE CPD PRODUCTION

The relative CPD production was used to assess the DNA damage in the UV-B irradiated cells. The DNA was extracted using TIANamp Bacteria DNA Kit (TIANGEN, China). The concentrations of DNA were determined by the absorbance at 260 nm and calculated by Lambert-beer law. In order to generate a uniform comparison, each DNA sample was diluted to 1 μg/mL. For enzyme-linked immunosorbent assay, first, 0.04% protamine sulfate was coated to a polyvinylchloride flat-bottomed microtitre plate for 2 h at 37°C. Fifty microliters of the denatured DNA were put into the plate wells and incubated for 1 h at 90°C. The plate was washed 5 times by phosphate-buffered saline with

twain (PBS-T) after drying. Then 200 μL of 3% BSA were add to each well and incubated at 37°C for 30 min and washed as described above. After blocking, 100 μL anti-thymine dimer antibody [H3] (abcam, USA) were added and incubated at 37°C for 1 h, then washed again. The plate with 100 μL/well HRP affinipure goat anti-mouse IgG (EarthOx, USA) was incubated at 37°C for 30 min. Then, the plate was washed 3 times with PBS-T and 2 times with citrate-phosphate buffer of pH 5.0. Finally, 100 μL of o-phenylene diamine and 0.007% hydrogen peroxide in citrate-phosphate buffer were then added to each well and incubated for 30 min at 37°C. Fifty microliters of 2 mol/L H_2SO_4 were added to stop the reactions. The absorbance was then read at 490 nm using a microplate reader (SynergyTMH4, BioTek, USA) to determine the CPD photoproduct. The relative generations of CPD were normalized by the absorbance of the blank control.

DETECTION OF ROS GENERATION

The generation of ROS was analyzed by using DCFH-DA method based on previous report (He and Häder, 2002). DCFH-DA can be taken by cell and hydrolyzed to DCFH, which can not pass through cell membranes and is trapped within cell. Intracellular ROS can oxidize nonfluorescent DCFH into DCF, a highly fluorescent compound. Here, after irradiation, 2 mM 5 μL DCFH-DA were immediately added to 200 μL of the irradiated samples and incubated at 37°C for 30 min in dark. The fluorescence of the samples was measured using a spectrofluorometer (SynergyTMH4, BioTek, USA) with the excitation wavelength of 488 nm and emission wave lengths between 500 and 600 nm. The fluorescence intensity at 525 nm, after subtraction of the fluorescence of blank control then normalizing to the protein content, was used to determine the relative ROS contents. Protein content was obtained by BCA protein assay kit (Thermo Scientific, USA).

CELLS AND MAGNETOSOMES ANALYSES

Morphologies of cells and magnetosome crystals of irradiated AMB-1 were analyzed using a JEOL JEM-1400 transmission electron microscope (TEM) with an accelerating voltage of 80 kV. About 20 μL of cells were dropped onto a copper TEM grid covered with carbon-coated formvar film for 2 h, then washed twice with sterilized distilled water and dried in air. Magnetosome sizes

were defined as (length + width)/2, and the shape factors as width/length by measuring TEM micrographs.

For rock magnetic measurements, the cells were harvested by centrifugation at 4°C. To prevent possible oxidation, the cell pellets were immediately transferred into a COY anaerobic chamber [$(O_2) < 300$ ppm, COY-7000220A, USA] and loaded into nonmagnetic gelatin capsules and dried for overnight. The samples were stored in $-20°C$ with N_2 protection prior to measurements (Li and Pan, 2012). Room temperature magnetic measurements were performed on a Model 3900 vibrating sample magnetometer (Princeton Measurements Corporation, USA, sensitivity 5.0×10^{-10} Am^2). Hysteresis loops were measured between $\pm$ 300 mT in 3 mT increments with 500 ms averaging time. The hysteresis parameters saturation magnetization (M_s), saturation remanence (M_{rs}), and coercivity (B_c) were determined after paramagnetic correction. Remanence coercivity (B_{cr}) was determined from a back-field demagnetization of the saturation isothermal remanent magnetization (SIRM) acquiring at 1.5 T field. First-order reversal curves (FORCs) were measured and calculated using the FORCinel version 1.22 software (Roberts et al., 2000; Harrison and Feinberg, 2008; Egli et al., 2010). The median coercivity ($B_{c, FORC}$) and half-width interaction field ($B_{b, 1/2}$) were calculated (Muxworthy and Dunlop, 2002; Winklhofer and Zimanyi, 2006; Li et al., 2013b).

Low-temperature magnetic measurements were performed on a Quantum Design Magnetic Property Measurement System (MPMS XP-5). Zero-field cooling (ZFC) and field cooling (FC) curves were acquired by first cooling the samples from 300 to 10 K in a zero field and in a 2.5 T field, respectively, and then measuring the demagnetization of remanence in zero field during warming from 10 to 300 K. The Verwey transition temperature (T_v) were determined as the temperature for the maximum value of the first derivative of the FC curves. The δ-ratio (δ_{FC}/δ_{ZFC}), where $\delta = (M_{80K} - M_{150K})/M_{80K}$, were calculated according to Moskowitz et al. (1993).

RESULTS

THE CELL GROWTH AFTER UV-B IRRADIATION

The effect of UV-B radiation on cell growth indicates a clear dose dependence as revealed by OD_{600} (**Figure 2**). The initial OD_{600} values of all samples were about 0.025 after re-suspending
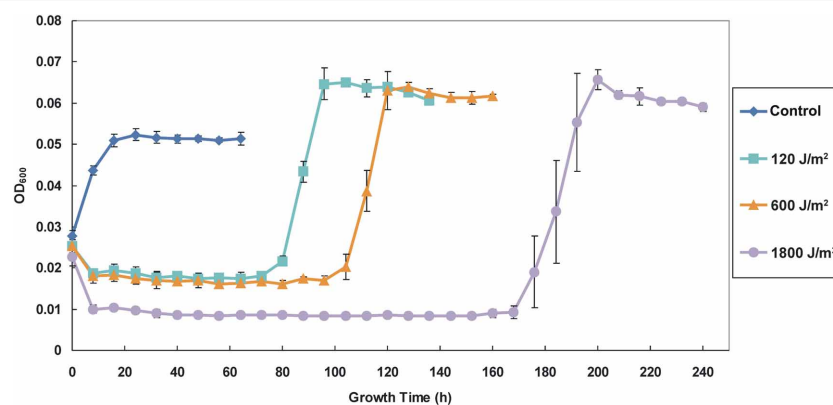

FIGURE 2 | Growth curves of the control (non-irradiated) and the irradiated AMB-1 cells. The diamond, square, triangle and circle shaped lines indicate the growth density (determine as OD_{600}) of the control and irradiated cells after 120, 600, and 1800 J/m^2 irradiation.

the irradiated cells in fresh medium. After the first 8 h following re-suspension, the cell concentrations of the 120, 600, and 1800 J/m^2 irradiated samples slightly decreased to 0.019, 0.018, and 0.01, respectively, which indicates differing degrees of cell density loss. Subsequently, before they reached exponent growth phases and stationary phases, the irradiated samples remained relatively stable at low levels cell density (static phase or recovery time) for 72, 96, and 168 h for the groups received 120, 600, and 1800 J/m^2 irradiation, respectively. The non-irradiated control group exhibited rapid growth after re-suspension and reached constant at stationary phase within 24 h. We also note that the 1800 J/m^2 irradiation group had the longest recovery period and the largest standard deviation during growing at exponent phase, which suggests that the higher dose of irradiation might have caused more damage to cells in this group. Compared with the control group, all irradiated groups had a relatively higher OD_{600} in the stationary phase after recovery.

VARIATIONS OF THE CPD FORMATION AND THE ROS ACCUMULATION

As expected, UV-B radiation caused significant deleterious effects on DNA and cellular levels that correspond to the generation of CPD and the accumulation of ROS, respectively, which also exhibited dose-dependent patterns (**Figure 3**). CPD, induced by UV-B photons, is a photoproduct known as DNA lesions, which can blocks DNA replication and transcription. ROS is a collection of superoxide radical (O_2^{-}), hydroxylradial ($OH^{\cdot}$), hydrogen peroxide (H_2O_2) and singlet oxygen ($^1O_2$) (He and Häder, 2002). These free radicals can lead to damages of lipids, proteins, and DNA. In our experiments, the strain AMB-1 exhibited distinct detrimental effects under different levels of UV-B irradiation.

Specifically, for the control, 120, 600, and 1800 J/m^2 groups, the amount of relative CPD generation were 0.118 ± 0.018, 0.133 ± 0.037, 0.599 ± 0.023, and 0.680 ± 0.011, while the ROS value reached 24.07 ± 1.79, 36.81 ± 5.58, 74.33 ± 7.37, and 98.66 ± 1.22 (determined by normalized relative units), respectively.

CHANGES OF THE CELL SIZE, MAGNETOSOMES AND CHAIN STRUCTURES

The detailed information of the AMB-1 cells and magnetosomes after the bacteria recovered from UV-B irradiation are summarized in **Table 1**. **Figures 4A–D** are representative TEM micrographs of the AMB-1 cells of the four experiment groups. Interestingly, all UV-B irradiated cells produced larger grain sizes and longer magnetosome chains compared with the non-irradiated cells. Statistic analyses of each group indicate that the magnetosome grain size of the irradiated cells was nearly 10 nm larger on average than the non-irradiated cells. For the irradiated groups, we noticed decreased number of subchains per cell (N_s), increased number of magnetosomes per cell (N_m) and per subchain (N_{sm}) (**Table 2**). However, the average cell lengths of the irradiated cells were about 0.4 μm shorter than the control group. Although all irradiated samples had differences in cell size and magnetosome parameters, no clear dose-related change trend was observed.

THE COERCIVITY, FORC DIAGRAMS AND δ-RATIOS

Magnetic properties of the whole cell samples were displayed in **Table 2** and **Figure 5**. Consistent with previous studies on whole-cell MTB samples, all samples were characterized by Stoner-Wohlfath-type hysteresis loops with M_{rs}/M_s ratio close to 0.5 (Stoner and Wohlfarth, 1948), and central-ridged FORC
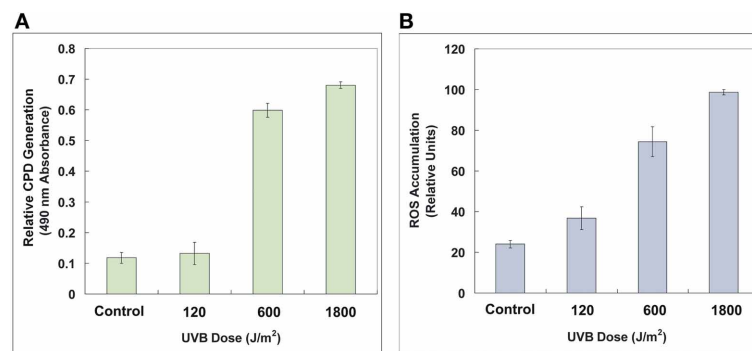

FIGURE 3 | Relative CPD generation (A) and ROS accumulation (B) of the control and the irradiated AMB-1 cells. The CPD formation was determined by 490 nm absorbance. The ROS content was characterized by 525 nm fluorescent intensity normalized protein content. See text for details.

Table 1 | Cell length, magnetosome, and subchain information of the AMB-1 samples at different irradiation levels.

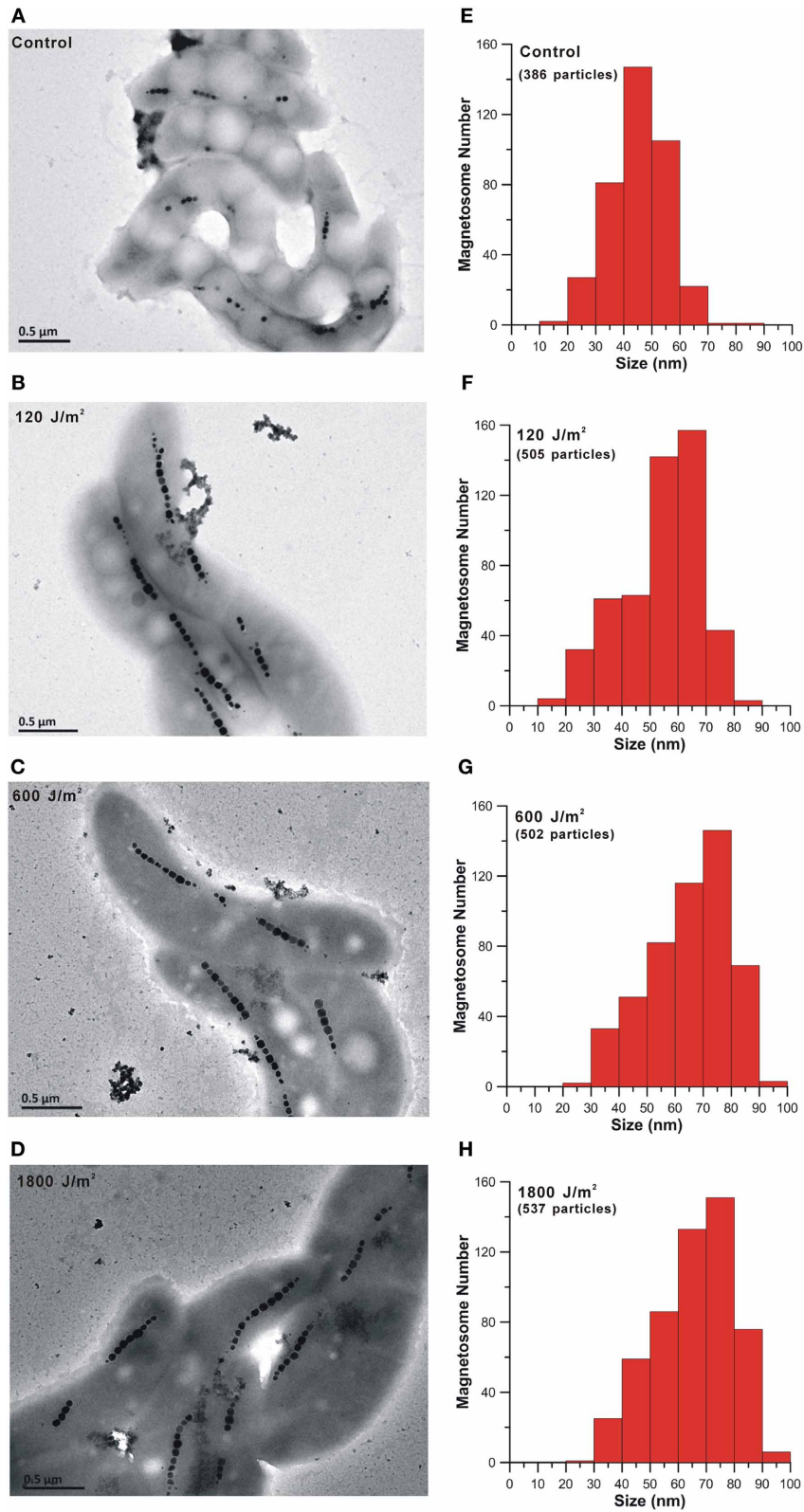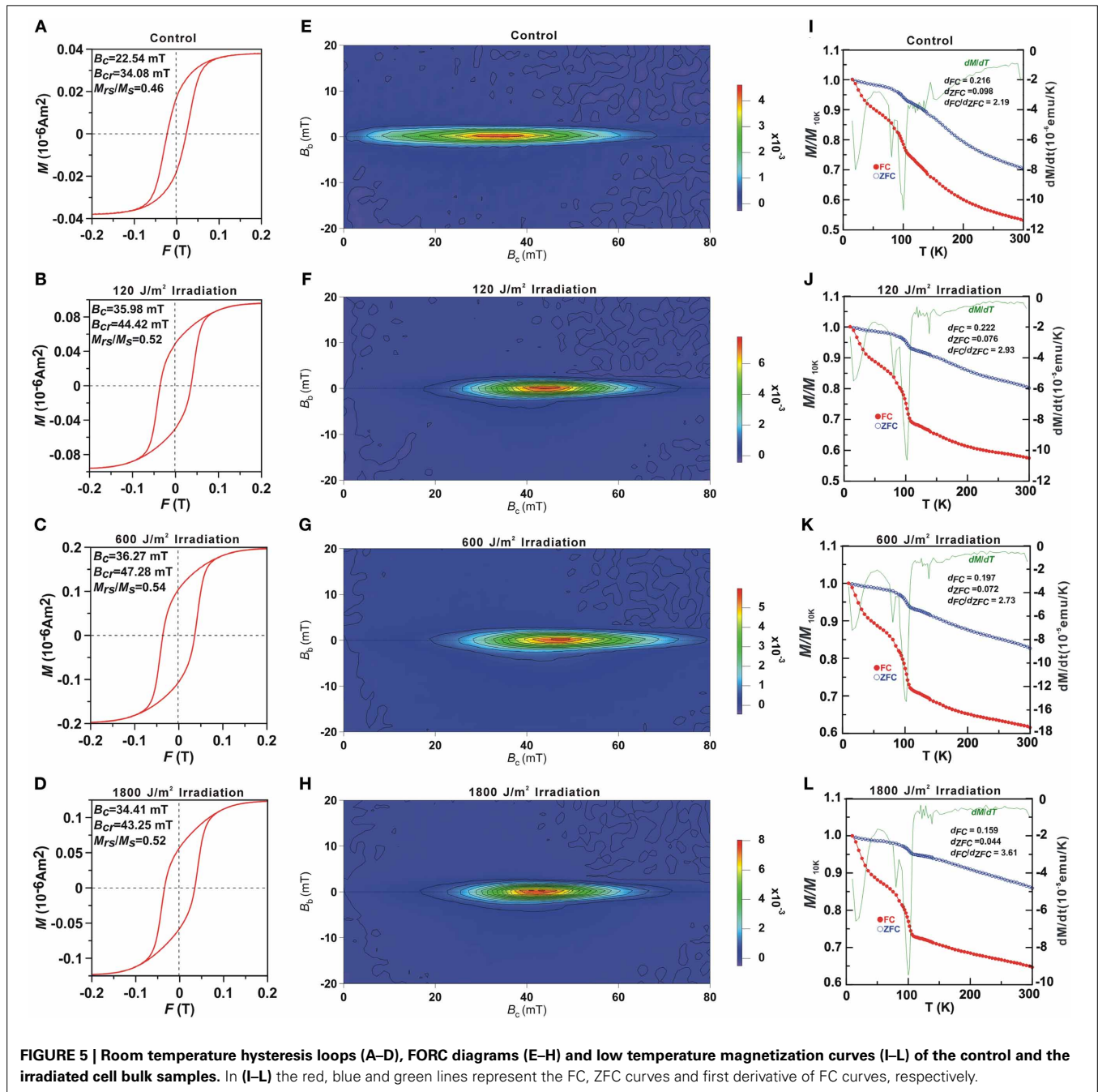| UV-B dose (J/m^2)	Cell length(μm)	Magnetosome			Magnetosome chain	
		Size (nm)	Shape factor	N_m (per cell)	N_s (per cell)	N_{sm} (per subchain)
Control	3.01 ± 0.41	45.44 ± 10.31	0.913 ± 0.077	11 ± 3	3 ± 1	3 ± 2
120	2.64 ± 0.65	54.24 ± 13.84	0.860 ± 0.088	20 ± 6	2 ± 1	10 ± 4
600	2.56 ± 0.38	55.43 ± 14.43	0.857 ± 0.089	19 ± 5	2 ± 1	9 ± 3
1800	2.61 ± 0.43	55.79 ± 13.78	0.859 ± 0.085	21 ± 5	2 ± 1	10 ± 4

FIGURE 4 | TEM micrographs of cell morphology and magnetosome chains and histograms of magnetosome grain sizes of the control (A and E) and the irradiated AMB-1 cells (B–D and F–H).

Table 2 | Magnetic parameters of the bulk AMB-1 samples at different irradiation levels.

UV-B dose (J/m^2)	B_c (mT)	B_{cr} (mT)	B_{cr}/B_c	M_{rs}/M_s	$B_{c, FORC}$ (mT)	$B_{b1/2}$ (mT)	T_v (K)	δ_{FC}	δ_{ZFC}	δ_{FC}/δ_{ZFC}
Control	22.54	34.08	1.51	0.46	34.9	1.31	102	0.216	0.098	2.19
120	35.98	44.42	1.23	0.52	43.6	1.41	102	0.222	0.076	2.93
600	36.27	47.28	1.30	0.54	46.0	1.51	102	0.197	0.072	2.73
1800	34.41	43.25	1.26	0.52	43.4	1.41	102	0.159	0.044	3.61

FIGURE 5 | Room temperature hysteresis loops (A–D), FORC diagrams (E–H) and low temperature magnetization curves (I–L) of the control and the irradiated cell bulk samples. In **(I–L)** the red, blue and green lines represent the FC, ZFC curves and first derivative of FC curves, respectively.

diagrams characterized with a narrow distributed along B_c axis (**Figures 5E–H**), indicating non-interacting uniaxial SD assemblages (Egli et al., 2010). In comparison, the room temperature magnetic parameters B_c, B_{cr} and, B_c, FORC of the UV-B radiation-treated samples were nearly identical, but about 10 mT higher than the control group. The decreased B_{cr}/B_c values, increased M_{rs}/M_s values and right-shifted FORCs suggest that the radiation treated samples possess magnetite crystals with larger grain sizes and/or longer chains, which have also been confirmed by the TEM observations (**Figure 4**).

Low-temperature measurements (**Figures 5I–L**) showed that the magnetic remanence of the UV-B radiation treated cells decreased rapidly at both ∼15–30 and ∼102 K in FC curves. The T_v of 102 K was similar to previous reports of magnetosome produced by strain AMB-1 (e.g., Li et al., 2009), which indicates no distinct change in the magnetosome composition by irradiation treatment. The δ-ratio of the control, 120, 600, and 1800 J/m^2 irradiated samples were 2.10, 2.93, 2.73, and 3.61, respectively, which further demonstrates better magnetosome chain structures in the radiation treated groups (Moskowitz et al., 1993).

DISCUSSION

THE BIOLOGICAL DELETERIOUS EFFECTS OF UV-B IRRADIATION ON AMB-1 CELLS

In this study, *M. magneticum* AMB-1 was used as a model organism to probe the UV-B biological effects on the cell growth and biomineralization. We found an initial decrease of cell density (OD_{600}) and a significant inhibition of growth of the AMB-1 after the bacteria were irradiated under doses of 120, 600, and 1800 J/m^2 (**Figure 2**). The increased CPD formation and the ROS accumulation (**Figure 3**) indicated clearly UV-B dose-dependent deleterious effects on both DNA and cellular levels after UV-B irradiation. The self-repair after UV-B radiation might cause the observed prolonged static period of irradiated AMB-1 cells (Agogué et al., 2005; Goosen and Moolenaar, 2008). However, after the cells fully recovered (40 h after reaching stationary growth phases), the accumulations of CPD were 0.075 ± 0.007, 0.086 ± 0.027, 0.092 ± 0.036 and 0.088 ± 0.033, and the ROS values were 31.45 ± 5.48, 25.76 ± 3.56, 30.04 ± 8.31, and 30.50 ± 3.64 for the control, 120, 600, and 1800 J/m^2 irradiated groups, respectively. Those values of the irradiated groups were comparable to the non-irradiated control group, which suggests that AMB-1 cells are able to repair the UV-B radiation damage.

Previous studies on repair strategies of aquatic organisms have demonstrated that after UV-B irradiation bacteria displayed a high efficient DNA light and dark repair to eliminate CPD that would block the replication and transcriptional process and lethiferous (Goosen and Moolenaar, 2008). For ROS that leads to cell membrane damage and cellular injuries, a series of antioxidant enzyme (e.g., superoxide dismutase, catalase, and peroxidase) can be induced to mitigate the negative effects caused by ROS (He and Häder, 2002; Xie et al., 2009; Santos et al., 2012). Transcriptome analysis of UV irradiated bacteria such as *Deinococcus* sp. and cyanobacterium *Synechocystis* also exhibited the up regulation of DNA repair and stress response-related genes. Both base/nucleotide excision repair and recombinational repair pathway participated in UV induced damage repair. Genes that were involved in scavenging oxygen radicals were also noticed up regulated after UV irradiation (Reid and Isaksen, 1976; Huang et al., 2002; Qiu et al., 2005a,b; Yuan et al., 2012).

Except for high efficiency removal of toxic oxygen species and specialized light and dark repair systems, other abilities (e.g., positive migration and production of UV screening pigments and compounds) can also help bacteria in avoiding harmful UV radiation (Ehling-Schulz and Scherer, 1999; Goosen and Moolenaar, 2008; Singh et al., 2010). Compared with non-magnetotactic bacteria in nature, MTB may migrate efficiently to deeper water layer or into sediments to avoid harmful UV radiation owing to their unique magnetotaxis. In addition, magnetite/greigite crystals may protect MTB from UV radiation.

POSSIBLE EFFECTS ON MAGNETOSOME BIOMINERALIZATION

TEM observations revealed that the irradiated cells, with a prolonged static phase, synthesized more and larger magnetosomes, as well as longer chains, which were further confirmed by various rock magnetic measurements. All irradiated samples had higher B_c, B_{cr}, M_s, M_{rs} and δ-ratio, and the FORC diagrams exhibited right shifts. Increased B_c, B_{cr} and B_c, FORC were largely due to the increased magnetosome chain lengths and grain sizes, while higher M_s and M_{rs} were probably caused by increased magnetosome production, consistent with previous studies on magnetite particles within the SD range (Kobayashi et al., 2006; Kopp and Kirschvink, 2008; Li et al., 2009). When we reinoculated these irradiated but fully recovered cells into the same fresh medium once more, however, no enhancement of magnetosome biomineralization was detected in the stationary phases compared with the non-irradiated group. This suggests that the observed enhanced magnetite biomineralization maybe the regulation induced by irradiation rather than a genetic imprint or radiation selection under the used experimental condition for AMB-1. Some self-repair processes and related metabolism changes may influence the crystallization of magnetosomes as well. At this stage, we cannot exclude that the prolonged recovery time of irradiated cells might affect the magnetite magnetosome formation.

Magnetite magnetosome biomineralization of MTB have been well documented by the molecular biologists and mineralogists (Bazylinski et al., 2007; Faivre and Schüler, 2008; Pósfai and Dunin-Borkowski, 2009). Previous studies have shown that biomineralization of chain arranged magnetite magnetosomes undergo several steps: formation of membrane vesicles on filamentary skeleton, iron uptake and magnetite crystallization within magnetosome membrane (Komeili, 2012). It has been found that the synthesis of magnetite magnetosome was closely related to nitrate reduction pathway (Bazylinski and Blakemore, 1983; Ge et al., 2011; Wang et al., 2011; Li et al., 2012). Iron and oxygen metabolism regulation also had significant influences on biomineralization of the cultured MSR-1 strain (Qi et al., 2012; Rong et al., 2012). Based on TEM micrographs, in addition to the magnetosome changes, the irradiated groups possess less round granules (possibly PHA which described by Keim et al., 2005; Silva et al., 2008) than the non-irradiated control group (data not shown). This is likely caused by the prolonged cell growth or some potential modification in the metabolism pathways within the irradiated cells. It also implies

that the UV-B radiation may induce metabolism changes in AMB-1, which in turn affects magnetosome biomineralization. This suggestion is also supported by previous reports that UV radiation can strongly affect the metabolism of other microorganisms. For example, up regulated nitrate reduction genes such as *nap* and *nos* genes and genes related to iron-sequestering (*bpc* and *hem*H) and peroxide metabolism (e.g., *oxy*R, *kat*G, and *sod*B) were verified through transcriptome analyses of both radio-resistant bacterium *Deinococcus* species and a facultative anaerobic *Gammaproteobacteria Shewanella oneidensis* MR-1 after UV irradiation (Qiu et al., 2005a,b). Nevertheless, further investigations on time-series culture medium composition analyses and transcriptome of the irradiated AMB-1 cells are needed to reveal the mechanisms of these phenomena.

It is reasonable to assume that the enhanced biomineralization of magnetosomes in MTB may have some benefits for resistance of irradiation. The large size, number, and improved chain structures of magnetosomes in the MTB cell may greatly help bacteria to mitigate damage caused by UV-B. For example, the magnetosomes themselves are able to prevent the radiation and eliminate intracellular ROS (Guo et al., 2012). Moreover, the better magnetite magnetosome formation in cells may enhance the sensibility of magnetotaxis navigation to escape from UV exposure when magnetic field is low. A deep-branching group MTB, affiliating within the *Nitrospira* phylum, which contains a few hundred to a thousand bullet-shaped magnetite magnetosomes, are widely found in aquatic environments (Spring et al., 1993; Pan et al., 2005; Li et al., 2010; Jogler et al., 2011; Lin et al., 2012). Our new data support that the synthesis of large amount of magnetosomes within one cell might be significant evolutionary benefit for such MTB that lived on early Earth as the geomagnetic field was probably weak and the UV radiation was strong.

SUPPLEMENTARY MATERIAL

The Supplementary Material for this article can be found online at: http://www.frontiersin.org/journal/10.3389/fmicb.2013.00397/abstract

REFERENCES

Agogué, H., Joux, F., Obernosterer, I., and Lebaron, P. (2005). Resistance of marine bacterioneuston to solar radiation. *Appl. Environ. Microbiol.* 71, 5282–5289. doi: 10.1128/AEM.71.9.5282-5289.2005

Arató, B., Szányi, Z., Flies, C., Schüler, D., Frankel, R. B., Buseck, P. R., et al. (2005). Crystal-size and shape distributions of magnetite from uncultured magnetotactic bacteria as a potential biomarker. *Am. Mineral.* 90, 1233–1240. doi: 10.2138/am.2005.1778

Bazylinski, D. A., and Blakemore, R. (1983). Denitrification and assimilatory nitrate reduction in *Aquaspirillum magnetotacticum*. *Appl. Environ. Microbiol.* 46, 1118–1124.

Bazylinski, D. A., and Frankel, R. B. (2004). Magnetosome formation in prokaryotes. *Nat. Rev. Microbiol.* 2, 217–230. doi: 10.1038/nrmicro842

Bazylinski, D. A., Frankel, R. B., and Konhauser, K. O. (2007). Modes of biomineralization of magnetite by microbes. *Geomicrobiol. J.* 24, 465–475. doi: 10.1080/01490450701572259

Blakemore, R., Maratea, D., and Wolfe, R. (1979). Isolation and pure culture of a freshwater magnetic spirillum in chemically defined medium. *J. Bacteriol.* 140, 720–729.

Chang, S. B. R., and Kirschvink, J. L. (1989). Magnetofossils, the magnetization of sediments, and the evolution of magnetite biomineralization. *Annu. Rev. Earth Planet. Sci.* 17, 169. doi: 10.1146/annurev.ea.17.050189.001125

Cockell, C. S. (1998). Biological effects of high ultraviolet radiation on early Earth-a theoretical evaluation. *J. Theor. Biol.* 193, 717–729. doi: 10.1006/jtbi.1998.0738

Egli, R., Chen, A. P., Winklhofer, M., Kodama, K. P., and Horng, C. S. (2010). Detection of noninteracting single domain particles using first-order reversal curve diagrams. *Geochem. Geophys. Geosyst.* 11, Q01Z11. doi: 10.1029/2009GC002916

Ehling-Schulz, M., and Scherer, S. (1999). UV protection in cyanobacteria. *Eur. J. Phycol.* 34, 329–338. doi: 10.1080/09670269910001736392

Faivre, D., Menguy, N., Pósfai, M., and Schüler, D. (2008). Environmental parameters affect the physical properties of fast-growing magnetosomes. *Am. Mineral.* 93, 463–469. doi: 10.2138/am.2008.2678

Faivre, D., and Schüler, D. (2008). Magnetotactic bacteria and magnetosomes. *Chem. Rev.* 108, 4875. doi: 10.1021/cr078258w

Garcia-Pichel, F. (1998). Solar ultraviolet and the evolutionary history of cyanobacteria. *Orig. Life Evol. Biosph.* 28, 321–347. doi: 10.1023/A:1006545303412

Ge, X., Wang, K., Bo, T., Kou, Y., Liu, W., and Chen, G. (2011). *Magnetospirillum magneticum* AMB-1 peroxiredoxins contribute to the aerotolerance and genetic stability of the genomic magnetosome island. *FEMS Microbiol. Lett.* 320, 118–127. doi: 10.1111/j.1574-6968.2011.02298.x

Glassmeier, K. H., and Vogt, J. (2010). Magnetic polarity transitions and biospheric effects. *Space Sci. Rev.* 155, 387–410. doi: 10.1007/s11214-010-9659-6

Goosen, N., and Moolenaar, G. F. (2008). Repair of UV damage in bacteria. *DNA Repair* 7, 353–379. doi: 10.1016/j.dnarep.2007.09.002

Guo, F. F., Yang, W., Jiang, W., Geng, S., Peng, T., and Li, J. L. (2012). Magnetosomes eliminate intracellular reactive oxygen species in *Magnetospirillum gryphiswaldense* MSR-1. *Environ. Microbiol.* 14, 1722–1729. doi: 10.1111/j.1462-2920.2012.02707.x

Häder, D. P., Kumar, H., Smith, R., and Worrest, R. (2007). Effects of solar UV radiation on aquatic ecosystems and interactions with climate change. *Photochem. Photobiol. Sci.* 6, 267–285. doi: 10.1039/b700020k

Hargreaves, B. R. (2003). "Water column optics and penetration of UVR," in *UV Effects in Aquatic Organisms and Ecosystems*, eds E. W. Helbling and H. Zagarese (London: The Royal Society of Chemistry), 59–105. doi: 10.1039/9781847552266-00059

Harrison, R. J., and Feinberg, J. M. (2008). FORCinel: an improved algorithm for calculating first-order reversal curve distributions using locally weighted regression smoothing. *Geochem. Geophys. Geosyst.* 9, Q05016. doi: 10.1029/2008GC001987

He, Y. Y., and Häder, D. P. (2002). Involvement of reactive oxygen species in the UV-B damage to the cyanobacterium *Anabaena* sp. *J. Photochem. Photobiol. B* 66, 73–80. doi: 10.1016/S1011-1344(01)00278-0

Hernandez, E. A., Ferreyra, G. A., and Mac Cormack, W. P. (2006). Response of two Antarctic marine bacteria to different natural UV radiation doses and wavelengths. *Antarct. Sci.* 18, 205–212. doi: 10.1017/S0954102006000241

Huang, L., McCluskey, M. P., Ni, H., and LaRossa, R. A. (2002). Global gene expression profiles of the cyanobacterium *Synechocystis* sp. strain PCC 6803 in response to irradiation with UV-B and white light. *J. Bacteriol.* 184, 6845–6858. doi: 10.1128/JB.184.24.6845-6858.2002

Jogler, C., Wanner, G., Kolinko, S., Niebler, M., Amann, R., Petersen, N., et al. (2011). Conservation of proteobacterial magnetosome genes and structures in an uncultivated member of the deep-branching *Nitrospira* phylum. *Proc. Natl. Acad. Sci. U.S.A.* 108, 1134–1139. doi: 10.1073/pnas.1012694108

Keim, C. N., Solórzano, G., Farina, M., and Lins, U. (2005). Intracellular inclusions of uncultured magnetotactic bacteria. *Int. Microbiol.* 8, 111–117.

Kobayashi, A., Kirschvink, J. L., Nash, C. Z., Kopp, R. E., Sauer, D. A., Bertani, L. E., et al. (2006). Experimental observation of magnetosome chain collapse in magnetotactic bacteria: sedimentological, paleomagnetic, and evolutionary implications. *Earth Planet. Sci. Lett.* 245, 538–550. doi: 10.1016/j.epsl.2006.03.041

Komeili, A. (2012). Molecular mechanisms of compartmentalization and biomineralization in magnetotactic bacteria. *FEMS Microbiol. Rev.* 36, 232–255. doi: 10.1111/j.1574-6976.2011.00315.x

Konhauser, K. O., Amskold, L., Lalonde, S. V., Posth, N. R., Kappler, A., and Anbar, A. (2007). Decoupling photochemical Fe (II) oxidation from shallow-water BIF deposition. *Earth Planet. Sci. Lett.* 258, 87–100. doi: 10.1016/j.epsl.2007.03.026

Kopp, R. E., and Kirschvink, J. L. (2008). The identification and biogeochemical interpretation of fossil magnetotactic bacteria. *Earth Sci. Rev.* 86, 42–61. doi: 10.1016/j.earscirev.2007.08.001

Li, J., Benzerara, K., Bernard, S., and Beyssac, O. (2013a). The link between biomineralization and fossilization of bacteria: insights from field and experimental studies. *Chem. Geol.* 359, 49–69. doi: 10.1016/j.chemgeo.2013.09.013

Li, J., Ge, K., Pan, Y., Williams, W., Liu, Q., and Qin, H. (2013b). A strong angular dependence of magnetic properties of magnetosome chains: implications for rock magnetism and paleomagnetism. *Geochem. Geophys. Geosyst.* 14, 3887–3907. doi: 10.1002/ggge.20228

Li, J., and Pan, Y. (2012). Environmental factors affect magnetite magnetosome synthesis in *Magnetospirillum magneticum* AMB-1: implications for biologically controlled mineralization. *Geomicrobiol. J.* 29, 362–373. doi: 10.1080/01490451.2011.565401

Li, J., Pan, Y., Chen, G., Liu, Q., Tian, L., and Lin, W. (2009). Magnetite magnetosome and fragmental chain formation of *Magnetospirillum magneticum* AMB-1: transmission electron microscopy and magnetic observations. *Geophys. J. Int.* 177, 33–42. doi: 10.1111/j.1365-246X.2009.04043.x

Li, J., Pan, Y., Liu, Q., Yu-Zhang, K., Menguy, N., Che, R., et al. (2010). Biomineralization, crystallography and magnetic properties of bullet-shaped magnetite magnetosomes in giant rod magnetotactic bacteria. *Earth Planet. Sci. Lett.* 293, 368–376. doi: 10.1016/j.epsl.2010.03.007

Li, Y., Katzmann, E., Borg, S., and Schüler, D. (2012). The periplasmic nitrate reductase Nap is required for anaerobic growth and involved in redox control of magnetite biomineralization in *Magnetospirillum gryphiswaldense*. *J. Bacteriol.* 194, 4847–4856. doi: 10.1128/JB.00903-12

Lin, W., Li, J., and Pan, Y. (2012). Newly isolated but uncultivated magnetotactic bacterium of the phylum *Nitrospirae* from Beijing, China. *Appl. Environ. Microbiol.* 78, 668–675. doi: 10.1128/AEM.06764-11

Lin, W., Wang, Y., Gorby, Y., Nealson, K., and Pan, Y. (2013a). Integrating niche-based process and spatial process in biogeography of magnetotactic bacteria. *Sci. Rep.* 3, 1643. doi: 10.1038/srep01643

Lin, W., Bazylinski, D. A., Xiao, T., Wu, L. F., and Pan, Y. (2013b). Life with compass: diversity and biogeography of magnetotactic bacteria. *Environ. Microbiol.* doi: 10.1111/1462-2920.12313. [Epub ahead of print].

Lin, W., Wang, Y., Li, B., and Pan, Y. (2011). A biogeographic distribution of magnetotactic bacteria influenced by salinity. *ISME J.* 6, 475–479. doi: 10.1038/ismej.2011.112

Lins, U., Keim, C. N., Evans, F. F., Farina, M., and Buseck, P. R. (2007). Magnetite (Fe_3O_4) and greigite (Fe_3S_4) crystals in multicellular magnetotactic prokaryotes. *Geomicrobiol. J.* 24, 43–50. doi: 10.1080/01490450601134317

Mandal, S., Rath, J., and Adhikary, S. P. (2011). Adaptation strategies of the sheathed *cyanobacterium Lyngbya majuscula* to ultraviolet-B. *J. Photochem. Photobiol. B* 102, 115–122. doi: 10.1016/j.jphotobiol.2010.09.011

Matallana-Surget, S., Joux, F., Wattiez, R., and Lebaron, P. (2012). Proteome analysis of the UVB-resistant marine bacterium *Photobacterium angustum* S14. *PLoS ONE* 7:e42299. doi: 10.1371/journal.pone.0042299

McKay, D. S., Gibson, E. K., Thomas-Keprta, K. L., Vali, H., Romanek, C. S., Clemett, S. J., et al. (1996). Search for past life on Mars: possible relic biogenic activity in Martian meteorite ALH84001. *Science* 273, 924–930. doi: 10.1126/science.273.5277.924

McKenzie, R. L., Björn, L. O., Bais, A., and Ilyasd, M. (2003). Changes in biologically active ultraviolet radiation reaching the Earth's surface. *Photochem. Photobioll. Sci.* 2, 5–15. doi: 10.1039/b211155c

Moskowitz, B. M., Frankel, R. B., and Bazylinski, D. A. (1993). Rock magnetic criteria for the detection of biogenic magnetite. *Earth Planet. Sci. Lett.* 120, 283–300. doi: 10.1016/0012-821X(93)90245-5

Muxworthy, A. R., and Dunlop, D. J. (2002). First-order reversal curve (FORC) diagrams for pseudo-single-domain magnetites at high temperature. *Earth Planet. Sci. Lett.* 203, 369–382. doi: 10.1016/S0012-821X(02)00880-4

Pan, Y., Lin, W., Li, J., Wu, W., Tian, L., Deng, C., et al. (2009). Reduced efficiency of magnetotaxis in magnetotactic coccoid bacteria in higher than geomagnetic fields. *Biophysic. J.* 97, 986–991. doi: 10.1016/j.bpj.2009.06.012

Pan, Y., Petersen, N., Davila, A. F., Zhang, L., Winklhofer, M., Liu, Q., et al. (2005). The detection of bacterial magnetite in recent sediments of Lake Chiemsee (southern Germany). *Earth Planet. Sci. Lett.* 232, 109–123. doi: 10.1016/j.epsl.2005.01.006

Paterson, A. G., Wang, Y., and Pan, Y. (2013). The fidelity of paleomagnetic records carried by magnetosome chains. *Earth Planet. Sci. Lett.* 383, 82–91. doi: 10.1016/j.epsl.2013.09.031

Petersen, N., von Dobeneck, T., and Vali, H. (1986). Fossil bacterial magnetite in deep-sea sediments from the South Atlantic Ocean. *Nature* 320, 611–615. doi: 10.1038/320611a0

Phoenix, V., Konhauser, K., Adams, D., and Bottrell, S. (2001). Role of biomineralization as an ultraviolet shield: implications for Archean life. *Geology* 29, 823–826. doi: 10.1130/0091-7613(2001)029<0823:ROBAAU>2.0.CO;2

Pósfai, M., and Dunin-Borkowski, R. E. (2009). Magnetic nanocrystals in organisms. *Elements* 5, 235–240. doi: 10.2113/gselements.5.4.235

Qi, L., Li, J., Zhang, W., Liu, J., Rong, C., Li, Y., et al. (2012). Fur in *Magnetospirillum gryphiswaldense* influences magnetosomes formation and directly regulates the genes involved in iron and oxygen metabolism. *PLoS ONE* 7:e29572. doi: 10.1371/journal.pone.0029572

Qiu, X., Tiedje, J. M., and Sundin, G. W. (2005a). Genome-wide examination of the natural solar radiation response in *Shewanella oneidensis* MR−1. *Photochem. Photobiol.* 81, 1559–1568. doi: 10.1562/2005-04-15-RA-490

Qiu, X., Sundin, G. W., Wu, L., Zhou, J., and Tiedje, J. M. (2005b). Comparative analysis of differentially expressed genes in *Shewanella oneidensis* MR-1 following exposure to UVC, UVB, and UVA radiation. *J. Bacteriol.* 187, 3556–3564. doi: 10.1128/JB.187.10.3556-3564.2005

Reid, G., and Isaksen, I. (1976). Influence of ancient solar-proton events on the evolution of life. *Nature* 259, 177–179. doi: 10.1038/259177a0

Roberts, A. P., Pike, C. R., and Verosub, K. L. (2000). First-order reversal curve diagrams: a new tool for characterizing the magnetic properties of natural samples. *J. Geophys. Res. Solid Earth.* 105, 28461–28476. doi: 10.1029/2000JB900326

Rong, C., Zhang, C., Zhang, Y., Qi, L., Yang, J., Guan, G., et al. (2012). FeoB2 functions in magnetosome formation and oxidative stress protection in *Magnetospirillum gryphiswaldense* strain MSR-1. *J. Bacteriol.* 194, 3972–3976. doi: 10.1128/JB.00382-12

Santos, A., Lopes, S., Baptista, I., Henriques, I., Gomes, N., Almeida, A., et al. (2011). Diversity in UV sensitivity and recovery potential among bacterioneuston and bacterioplankton isolates. *Lett. Appl. Microbiol.* 52, 360–366. doi: 10.1111/j.1472-765X.2011.03011.x

Santos, A. L., Gomes, N., Henriques, I., Almeida, A., Correia, A., and Cunha, Â. (2012). Contribution of reactive oxygen species to UV-B-induced damage in bacteria. *J. Photochem. Photobiol. B* 117, 40–46. doi: 10.1016/j.jphotobiol.2012.08.016

Santos, A. L., Oliveira, V., Baptista, I., Henriques, I., Gomes, N. C., Almeida, A., et al. (2013). Wavelength dependence of biological damage induced by UV radiation on bacteria. *Arch. Microbiol.* 195, 63–74. doi: 10.1007/s00203-012-0847-5

Schmidt, É. C., Scariot, L. A., Rover, T., and Bouzon, Z. L. (2009). Changes in ultrastructure and histochemistry of two red macroalgae strains of *Kappaphycus alvarezii* (*Rhodophyta, Gigartinales*), as a consequence of ultraviolet B radiation exposure. *Micron* 40, 860–869. doi: 10.1016/j.micron.2009.06.003

Silva, K. T., Abreu, F., Keim, C. N., Farina, M., and Lins, U. (2008). Ultrastructure and cytochemistry of lipid granules in the many-celled magnetotactic prokaryote, Candidatus *Magnetoglobus multicellularis*. *Micron* 39, 1387–1392. doi: 10.1016/j.micron.2008.05.009

Singh, S. P., Häder, D. P., and Sinha, R. P. (2010). Cyanobacteria and ultraviolet radiation (UVR) stress: mitigation strategies. *Ageing Res. Rev.* 9, 79–90. doi: 10.1016/j.arr.2009.05.004

Singh, V. P., Srivastava, P. K., and Prasad, S. M. (2012). Impact of low and high fluence rates of UV-B radiation on growth and oxidative stress in *Phormidium foveolarum* and *Nostoc muscorum* under copper toxicity: differential display of antioxidants system. *Acta Physiol. Plant.* 34, 2225–2239. doi: 10.1007/s11738-012-1023-x

Sinha, R. P., and Häder, D. P. (2008). UV-protectants in cyanobacteria. *Plant Sci.* 174, 278–289. doi: 10.1016/j.plantsci.2007.12.004

Solomon, S. (1999). Stratospheric ozone depletion: a review of concepts and history. *Rev. Geophys.* 37, 275–316. doi: 10.1029/1999RG900008

Spring, S., Amann, R., Ludwig, W., Schleifer, K. H., van Gemerden, H., and Petersen, N. (1993). Dominating role of an unusual magnetotactic bacterium in the microaerobic zone of a freshwater sediment. *Appl. Environ. Microbiol.* 59, 2397–2403.

Stadelmann, A., Vogt, J., Glassmeier, K. H., Kallenrode, M. B., and Voigt, G. H. (2010). Cosmic ray and solar energetic particle flux in paleomagnetospheres. *Earth Planets Space* 62, 333. doi: 10.5047/eps.2009.10.002

Stoner, E. C., and Wohlfarth, E. (1948). A mechanism of magnetic hysteresis in heterogeneous alloys. *Philos. T. R. Soc. A.* 240, 599–642. doi: 10.1098/rsta.1948.0007

Valet, J. P., and Valladas, H. (2010). The Laschamp-Mono lake geomagnetic events and the extinction of Neanderthal: a causal link or a coincidence? *Quaternary Sci. Rev.* 29, 3887–3893. doi: 10.1016/j.quascirev.2010.09.010

Wang, K., Ge, X., Bo, T., Chen, Q., Chen, G., and Liu, W. (2011). Interruption of the denitrification pathway influences cell growth and magnetosome formation in *Magnetospirillum magneticum* AMB-1. *Lett. Appl. Microbiol.* 53, 55–62. doi: 10.1111/j.1472-765X.2011.03063.x

Wang, Y., Lin, W., Li, J., and Pan, Y. (2013). High diversity of magnetotactic *deltaproteobacteria* in a freshwater niche. *Appl. Environ. Microbiol.* 79, 2813–2817. doi: 10.1128/AEM.03635-12

Weigand, M. R., and Sundin, G. W. (2009). Long-term effects of inducible mutagenic DNA repair on relative fitness and phenotypic diversification in *Pseudomonas cichorii* 302959. *Genetics* 181, 199–208. doi: 10.1534/genetics.108.096131

Weigand, M. R., and Sundin, G. W. (2012). General and inducible hypermutation facilitate parallel adaptation in *Pseudomonas aeruginosa* despite divergent mutation spectra. *Proc. Natl. Acad. Sci. U.S.A.* 109, 13680–13685. doi: 10.1073/pnas.1205357109

Weigand, M. R., Tran, V. N., and Sundin, G. W. (2011). Growth parameter components of adaptive specificity during experimental evolution of the uvr-inducible mutator *Pseudomonas cichorii* 302959. *PLoS ONE* 6:e15975. doi: 10.1371/journal.pone.0015975

Winklhofer, M., and Zimanyi, G. T. (2006). Extracting the intrinsic switching field distribution in perpendicular media: a comparative analysis. *J. Appl. Phys.* 99, 08E710–708E713. doi: 10.1063/1.2176598

Wulff, A., Roleda, M., Zacher, K., and Wiencke, C. (2008). UV radiation effects on pigments, photosynthetic efficiency and DNA of an Antarctic marine benthic diatom community. *Aquat. Biol.* 3, 167–177. doi: 10.3354/ab00076

Xie, Z., Wang, Y., Liu, Y., and Liu, Y. (2009). Ultraviolet-B exposure induces photo-oxidative damage and subsequent repair strategies in a desert cyanobacterium *Microcoleus vaginatus. Gom. Eur. J. Soil Biol.* 45, 377–382. doi: 10.1016/j.ejsobi.2009.04.003

Yamazaki, T., and Kawahata, H. (1998). Organic carbon flux controls the morphology of magnetofossils in marine sediments. *Geology* 26, 1064–1066.

Yuan, M., Chen, M., Zhang, W., Lu, W., Wang, J., Yang, M., et al. (2012). Genome sequence and transcriptome analysis of the radioresistant bacterium *Deinococcus gobiensis*: insights into the extreme environmental adaptations. *PLoS ONE* 7:e34458. doi: 10.1371/journal.pone.0034458

Zenoff, V. F., Sineriz, F., and Farías, M. (2006). Diverse responses to UV-B radiation and repair mechanisms of bacteria isolated from high-altitude aquatic environments. *Appl. Environ. Microbiol.* 72, 7857–7863. doi: 10.1128/AEM.01333-06

Zepp, R. G., Callaghan, T., and Erickson, D. (1998). Effects of enhanced solar ultraviolet radiation on biogeochemical cycles. *J. Photochem. Photobiol. B* 46, 69–82. doi: 10.1016/S1011-1344(98)00186-9